Applied Catalysis B: Environmental 95 (2010) 144–152

Contents lists available at ScienceDirect

Applied Catalysis B: Environmental

journal homepage: www.elsevier.com/locate/apcatb

Studies on surface structure of $M_xO_y/MoO_3/CeO_2$ system (M = Ni, Cu, Fe) and its influence on SCR of NO by NH_3

Jie Zhu [a], Fei Gao [b,*], Lihui Dong [a], Wujiang Yu [a], Lei Qi [a], Zhe Wang [a], Lin Dong [a,b,**], Yi Chen [a]

[a] Key Laboratory of Mesoscopic Chemistry of MOE, School of Chemistry and Chemical Engineering, Nanjing University, Nanjing 210093, PR China
[b] Center of Modern Analysis, Nanjing University, Nanjing 210093, PR China

ARTICLE INFO

Article history:
Received 8 July 2009
Received in revised form 15 December 2009
Accepted 18 December 2009
Available online 28 December 2009

Keywords:
Molybdena species
Surface structures
Acid sites
"NO + NH_3 + O_2"

ABSTRACT

MoO_3/CeO_2 and $M_xO_y/MoO_3/CeO_2$ (M = Fe, Cu, Ni) catalysts had been characterized by XRD, TPR, LRS, NH_3-adsorbed in situ FT-IR and activity test for selective catalytic reduction (SCR) of NO by NH_3. The results suggested that the addition of NiO, CuO and Fe_2O_3 to MoO_3/CeO_2 catalysts had led to the different structures of surface molybdena species, i.e., isolated regular tetrahedral, highly distorted tetrahedral and polymerized octahedral molybdena species, revealing that the intensities of interaction between molybdena species and these metal oxides could be listed as: $NiO/MoO_3/CeO_2 > CuO/MoO_3/CeO_2 > Fe_2O_3/MoO_3/CeO_2$. Furthermore, it exhibited the same order for the surface acid intensities of the Lewis acid sites of these samples. The reactivity of "NO + NH_3 + O_2" reaction is tightly related to acid properties of the catalysts (no matter Brønsted or Lewis acid sites): At low temperature, a weak Lewis acid site (L1) is the main active site for "NO + NH_3 + O_2" reaction; at middle temperature range, the Brønsted acid site is the primary active site; while at high temperature, another strong Lewis acid site (L2) can also promote the reaction.

1. Introduction

NO_x is the major source of air pollution, for it has the ability to generate secondary contaminants through its interactions with other primary pollutants [1]. In recent years, many methods have been used to reduce the emission of nitrogen oxide [2–11]. Among them, selective catalytic reduction (SCR) using transition metal oxides (supported/unsupported) catalysts with ammonia as the reducing agent is widely used for deNO_x in stationary pollution sources due to its high efficiency and has been investigated by many researchers [8–13]. The chemical and mechanistic aspects of NO reduction with ammonia ("NO + NH_3 + O_2" reaction) have been reviewed extensively and the surface acidity is considered to be tightly related with the reaction activity [12,13]. However, whether Brønsted or Lewis acid sites are active sites for this reaction is still controversial. Furthermore, almost all of these investigations are concerned with vanadia based catalysts. Comparatively, fewer reports can be found about the molybdena based catalysts [14–19]. Thus, it is meaningful to design a series of molybdena based catalysts with different acid sites and to investigate the correlation between surface acidity and the activity in the "NO + NH_3 + O_2" reaction.

As reported elsewhere, the surface acidity (Brønsted and Lewis acid sites) of Mo-based catalysts can be influenced by dropping various metal oxides, such as Ni, Co, etc. [20] Simultaneously, CeO_2 is an important support and has attracted more attention recently, due to its outstanding oxygen storage capacity and unique redox properties. Accordingly, it is promising to combine the advantages of Mo-based bimetallic oxides and ceria support.

Hence, in the present work, we prepared a series of bimetallic oxides (Ni–Mo, Cu–Ni and Fe–Mo) supported on ceria support. The surface states, reduction properties and acidity–basicity properties of the catalysts have been approached. In our previous work, we have long dedicated ourselves to the nature of the reaction. The catalytic activity tests, such as "CO + O_2" [21] and "NO + CO" [6,7], have been designed as model reactions in an ideal condition for better understanding the behaviors of the catalysts. Thus, here, a programming ideal model reaction for "NO + NH_3 + O_2" is applied to the catalysts with different acidity properties. The relationship between acid sites and activity has been suggested. In addition, a tentative model for the formation and the coordination environment of surface molybdena and M_xO_y species in $M_xO_y/MoO_3/CeO_2$ has been proposed.

* Corresponding author at: Center of Modern Analysis, Nanjing University, Nanjing 210093, PR China. Tel.: +86 25 83592290; fax: +86 25 83317761.
** Corresponding author at: Key Laboratory of Mesoscopic Chemistry of MOE, School of Chemistry and Chemical Engineering, Center of Modern Analysis, Nanjing University, Nanjing 210093, PR China. Tel.: +86 25 83592290; fax: +86 25 83317761.
E-mail addresses: gaofei@nju.edu.cn (F. Gao), donglin@nju.edu.cn (L. Dong).

0926-3373/$ – see front matter © 2009 Elsevier B.V. All rights reserved.
doi:10.1016/j.apcatb.2009.12.021

2. Experimental

2.1. Sample preparation

MoO_3 was pretreated at 450 °C in flowing air for 5 h before use. CeO_2 support, with a BET surface area of 59.6 m^2/g, was prepared by calcining $Ce(NO_3)_3{\cdot}6H_2O$ at 550 °C in flowing air for 5 h.

The MoO_3/CeO_2 samples were prepared by heating the mechanical mixtures with the required amounts of MoO_3 and CeO_2 at 450 °C in flowing air for 24 h. The samples were denoted as *x*Mo/Ce, e.g., 0.8Mo/Ce represents a sample with MoO_3 loading of 0.8 mmol/100 m^2 CeO_2.

The M_xO_y/CeO_2 (M = Ni, Cu, Fe) samples were prepared by impregnating CeO_2 supports with an aqueous solution containing required amounts of $Ni(NO_3)_2$, $Cu(NO_3)_2$ or $Fe(NO_3)_3$. The samples were dried at 100 °C for 12 h and then calcined at 450 °C in flowing air for 5 h. The loadings of M^{n+}(M = Ni, Cu, Fe) for all the samples were 0.3 mmol/100 m^2 CeO_2 and the samples were denoted as Ni/Ce, Cu/Ce and Fe/Ce, respectively.

The preparation method of $M_xO_y/MoO_3/CeO_2$ (M = Ni, Cu, Fe) was the same as M/Ce samples except the supports were 0.8Mo/Ce instead of CeO_2. The loadings of M^{n+} (M = Ni, Cu, Fe) for all the samples were 0.3 mmol/100 m^2 CeO_2 and the samples were denoted as Ni/Mo/Ce, Cu/Mo/Ce and Fe/Mo/Ce, respectively.

2.2. Characterization

X-ray diffraction (XRD) patterns were obtained with a Philips X'pert Pro diffractometer using Ni filtered Cu K_α radiation (0.15418 nm). The X-ray tube was operated at 40 kV and 40 mA.

Brunauer–Emmett–Teller (BET) surface area was measured by nitrogen adsorption at 77 K on a Micromeritics ASAP-2020 adsorption apparatus.

Laser Raman spectra (LRS) were recorded by using Renishaw Invia spectrometer. Raman excitation at 514.5 nm was provided by Ar^+ laser. A laser power of 20 mW was applied.

Temperature-programmed reduction (TPR) was carried out in a quartz U-tube reactor, and 100 mg sample was used for each measurement. Before reduction, the sample was pretreated in N_2 stream at 100 °C for 1 h and then cooled to room temperature. After that, a H_2–Ar mixture (7% H_2 by volume) with a flow rate of 40 mL min^{-1} was switched on and the temperature was increased linearly at a rate of 10 °C min^{-1}. A thermal conductivity cell was used to detect the consumption of H_2 on stream.

In situ Fourier-transform infrared spectroscopy (in situ FT-IR) of ammonia adsorption was carried out on a Nicolet 5700 FT-IR instrument (Thermo Electron Corporation, USA) running at 4 cm^{-1} resolutions. The nature of acid sites was investigated using ammonia as the probe molecule. A thin, but intact, self-supporting wafer (≈15 mg) of the adsorbents was prepared and mounted inside a high temperature cell (HTC-3, Harrick Scientific Corporation, USA). The wafer was pretreated by N_2 (99.999%) at 400 °C for 1 h. After cooling to ambient temperature, a stream of NH_3 (99.999%) with a flow rate of 5 mL min^{-1} was introduced into the HTC at atmospheric pressure for 30 min, then the cell was flushed by N_2 for 30 min. After that, the HTC was heated to 400 °C under N_2 atmosphere at a rate of 10 °C min^{-1} and the spectra were recorded at target temperatures.

The reaction activity tests of NO selective catalytic reduction by ammonia ("NO + NH_3 + O_2" reaction) were measured in a flow micro-reactor with a gas composition of 700 ppm NH_3, 700 ppm NO, 4% O_2 and 96% N_2 by volume at a space velocity of 180,000 mL g^{-1} h^{-1}, 50 mg catalyst was used for each measurement. The catalysts were tested at 200, 250, 300 and 350 °C, respectively, and the tail gas was analyzed by Saltzman method.

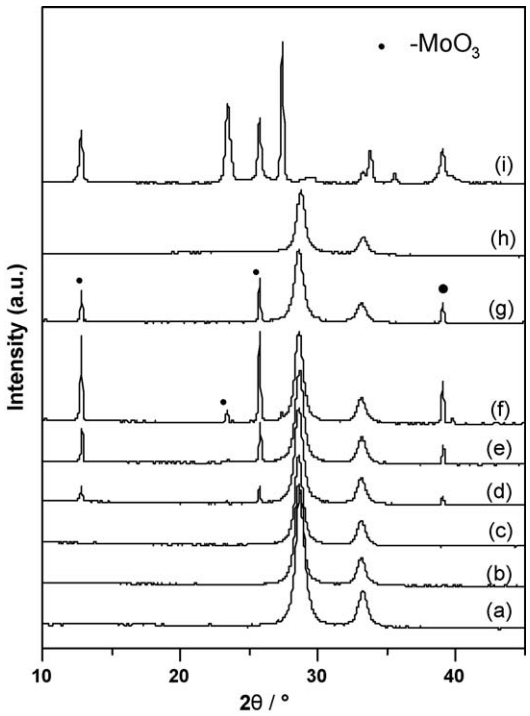

Fig. 1. XRD patterns of *x*Mo/Ce samples with different MoO_3 loadings. (a) 0.2, (b) 0.4, (c) 0.8, (d) 1.2, (e) 2.0, (f) 2.4 mmol/100 m^2 CeO_2, (g) uncalcined 0.2Mo/Ce, (h) pure CeO_2 and (i) pure MoO_3.

3. Results and discussion

3.1. XRD

Fig. 1 shows the XRD patterns of a series of Mo/Ce samples with different MoO_3 loadings. The XRD patterns of uncalcined 0.2Mo/Ce, pure CeO_2 and pure MoO_3 are also presented for comparison. For uncalcined 0.2Mo/Ce sample, the characteristic peaks of MoO_3 crystalline (typically at 2θ = 12.8°, 23.4°, 25.8°, 27.4° and 39.0°) can be observed in spite of low MoO_3 amount. After calcination, for those samples with low MoO_3 loadings (≤0.8 mmol/100 m^2 CeO_2), i.e., Fig. 1a–c with 0.2, 0.4 and 0.8 mmol/100 m^2 CeO_2, respectively, no characteristic peaks of crystalline MoO_3 have been observed, which suggests that MoO_3 species have been highly dispersed on the surface of CeO_2. However, characteristic peaks of crystalline MoO_3 have been found in high MoO_3 loading samples, as shown in Fig. 1d–f, and the intensities of the peaks increase with the increase of the MoO_3 loading, indicating some crystalline MoO_3 remain in these samples due to the high MoO_3 loading. As reported previously [22], the dispersion capacity of MoO_3 on the surface of CeO_2 is 0.8 mmol/100 m^2 and then the accompanying oxygen anions of Mo^{6+} form a close-packed monolayer of oxygen anions on the surface. Therefore, in our work, when the MoO_3 loading amount is 0.8 mmol/100 m^2, we can similarly consider the MoO_3 form monolayer on the surface of CeO_2 support.

Fig. 2 shows the XRD patterns of 0.8Mo/Ce and M/Mo/Ce (M = Ni, Cu, Fe) series samples. No any characteristic peaks of crystalline MoO_3 and metal oxides can be observed, indicating that the MoO_3 and M_xO_y exist as highly dispersed species for all the samples.

3.2. TPR

Shown in Fig. 3 are the TPR profiles of M/Mo/Ce series samples. It is clearly seen that the reduction temperatures of M_xO_y in M/Mo/Ce samples are much higher than corresponding M/Ce samples. For

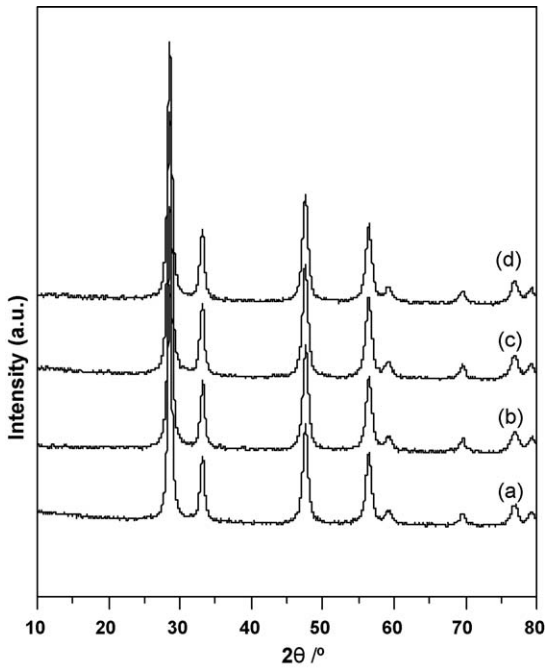

Fig. 2. XRD patterns of $M_xO_y/MoO_3/CeO_2$ samples with different M_xO_y loadings (M = Ni, Cu, Fe). (a) 0.8Mo/Ce, (b) Ni/Mo/Ce, (c) Cu/Mo/Ce and (d) Fe/Mo/Ce.

Ni/Ce sample (Fig. 3a), three hydrogen consumption peaks are observed. The peaks at about 226 and 268 °C can be ascribed to the reduction of adsorbed oxygen on the surface of ceria [23]. As reported in the literature [23], some Ni^{2+} ions can incorporate into the lattice of ceria and form solid solution. Therefore, the mismatch in ion size and charge amount of Ni^{2+} and Ce^{4+} leads to the lattice distortion and charge unbalance in ceria lattice. Thus, oxygen vacancies form and the Ni^{2+}-incorporated ceria are easily to adsorb oxygen atoms. As Ni^{2+} ions incorporated into solid solution are difficult to reduce, no reduction peaks corresponding to incorporated Ni^{2+} could be observed in experimental temperature range. The peak at about 300 °C is very weak, which could be ascribed to the reduction of dispersed NiO on the surface of ceria ($Ni^{2+} \rightarrow Ni^0$). While for Ni/Mo/Ce sample (Fig. 3b), the peak of $Ni^{2+} \rightarrow Ni^0$ shifts to higher temperature (364 °C) and no reduction peaks corresponding to adsorbed oxygen can be observed, indicating the interaction between NiO and CeO_2 is blocked by MoO_3 monolayer. Therefore, Ni^{2+} cannot incorporate into the ceria lattice.

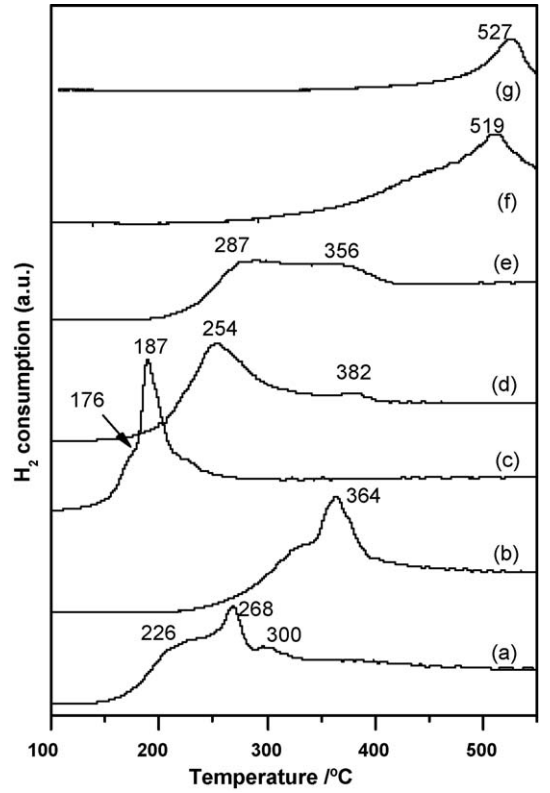

Fig. 3. TPR profiles of M_xO_y/CeO_2 and $M_xO_y/MoO_3/CeO_2$ samples. (a) Ni/Ce, (b) Ni/Mo/Ce, (c) Cu/Ce, (d) Cu/Mo/Ce, (e) Fe/Ce, (f) Fe/Mo/Ce and (g) 0.8Mo/Ce.

For Cu/Ce sample (Fig. 3c), the peaks at about 187 °C, with a shoulder at about 176 °C, are attributed to the stepwise reduction of surface dispersed CuO species, i.e., $Cu^{2+} \rightarrow Cu^+$ and $Cu^+ \rightarrow Cu^0$, respectively [24]. Moreover, only one reduction peak (~254 °C) is found in the TPR profile of Cu/Mo/Ce sample (Fig. 3d), and the reduction temperature is 67 °C higher than Cu/Ce sample. Mohamed [25] investigated silica supported copper–molybdenum catalysts. The results suggest that introducing of copper ions induces the formation of $CuMoO_4$ species. As no peaks attributed to any CuMo compounds could be observed in XRD patterns in our samples, it seems more reasonable to assume that for Cu/Mo/Ce catalysts, the CuO dispersed on the top of MoO_3 monolayer and the interaction of CuO and CeO_2 is blocked, leading to the elevation of reduction temperature of copper species compared with Cu/Ce sample. It also should be noted that a weak reduction peak appears at ~382 °C. Wang and Weng [26] studied the CuMoAl system and found that compared with MoAl sample, the reduction temperature of $Mo^{6+} \rightarrow Mo^{4+}$ shifts from 474 to 414 °C, indicating the CuO species promote the reduction of molybdena species. From the present study, it can be seen from the TPR curve of 0.8Mo/Ce sample (Fig. 3g) that a reduction peak at about 527 °C appears, which should be attributed to the reduction of $Mo^{6+} \rightarrow Mo^{4+}$. Thus, the peak at 382 °C might be attributed to the reduction of $Mo^{6+} \rightarrow Mo^{4+}$ on the surface of ceria promoted by CuO species.

For Fe/Ce and Fe/Mo/Ce samples (Fig. 3e and f), the Fe/Mo/Ce is more difficult to be reduced than Fe/Ce. The two peaks of Fe/Ce sample, centered at 287 and 356 °C, should be attributed to the Fe_2O_3 to Fe_3O_4 and Fe_3O_4 to FeO, respectively [27,28], while the reduction peak of Fe species in Fe/Mo/Ce sample is centered at ~519 °C.

Thus, from the TPR results, it can be considered that the Mo monolayer inhibits the reduction of metal oxides significantly for all the samples, indicating that the M_xO_y dispersed on the top of the MoO_3 monolayer, which may affect the coordination environment of metal ions greatly. Taking CuO as an example, as shown in Fig. 4a, the density of vacant sites available on the surface of ceria is about 1.22 mmol/100 m^2. As CuO disperses on ceria, the Cu^{2+} incorporates into the surface cubic vacant sites to form a comparatively unstable penta-coordinated structure, which is easy to be attacked by reductive molecules, such as H_2. When the ceria is modified by the monolayer dispersed MoO_3 species (0.8 mmol/100 m^2, Fig. 4b), about 2/3 surface vacant sites of ceria are occupied by Mo^{6+} and the capping oxygen ions of MoO_3 form a close-packed monolayer. For Cu/Mo/Ce sample, the Cu^{2+} ions of the dispersed copper oxide will incorporate into the tetrahedral vacant sites of the close-packed monolayer oxygen of MoO_3 to form a stable tetrahedral coordinated structure, which is difficult to be reduced. Meanwhile, as ceria has oxygen storage capacity, it has obvious promotion effects on Cu^{2+} reduction in Cu/Ce sample, while the interaction between CuO and CeO_2 is blocked in Cu/Mo/Ce sample, also leading to the higher reduction temperature. For Ni/Mo/Ce sample, similar explanations are applicable. Nevertheless, for Fe/Mo/Ce sample, as each Fe^{3+} needs 3/2 capping oxygen ions to reach charge balance, the coordination environment of Fe^{3+}

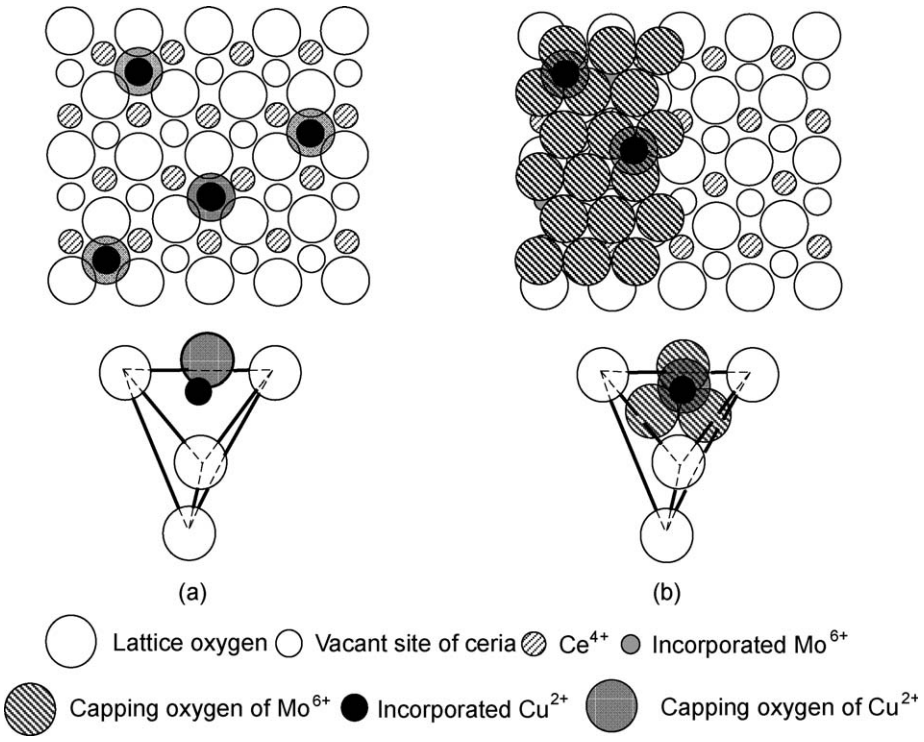

Fig. 4. Tentative model of surface Cu and molybdena species: (a) penta-coordinated Cu^{2+} species incorporated into the surface cubic vacant sites of ceria and (b) tetrahedrally coordinated Cu^{2+} species incorporated into the surface tetrahedral vacant sites of dispersed MoO_3.

might be unstable. In this situation, the MoO_3 monolayer blockage between Fe^{3+} and CeO_2 might be the dominative reason for higher reduction temperature.

3.3. LRS

The LRS spectra results of M/Mo/Ce samples ranging from 600 to 1100 cm^{-1} are presented in Fig. 5. As can be seen, no characteristic bands of crystalline MoO_3 (665, 818 and 995 cm^{-1}) can be observed for all the samples, indicating that the MoO_3 has been well dispersed on the surface of CeO_2. The result is consistent with XRD analysis. For 0.8Mo/Ce sample (Fig. 5a), two bands at about 805 and 965 cm^{-1} are detected, which are attributed to the stretching vibration of Mo–O–X (X = Mo or Ce) [29] and terminal Mo=O [30,31] of the surface molybdena species, respectively. After addition of M_xO_y (0.3 mmol/100 m^2), the frequencies of Mo–O–X keep almost unchanged (~800 cm^{-1}), while the frequencies of Mo=O bonds change differently, as shown in Fig. 5b–d. The peaks at about 956 cm^{-1} could be observed for all three samples, which are almost the same wave number compared with 0.8Mo/Ce sample. However, for Ni/Mo/Ce and Cu/Mo/Ce samples, another peak at about 872 cm^{-1} (Ni/Mo/Ce) and 904 cm^{-1} (Cu/Mo/Ce) attributed to the stretching vibration of Mo=O terminals could be observed, respectively, indicating a new structure of molybdena species forms on the surface of these two samples.

Many researchers have studied the relationship between the frequency of Mo=O terminals and the state of molybdena species dispersed on various supports by Raman spectra. As reported by Ng and Gulari [32], for MoO_3/TiO_2 samples, the Raman band at >955 cm^{-1} is attributed to the symmetric stretching mode of the Mo=O terminals in the surface polymeric octahedral molybdena species, while the Raman band at ≤955 cm^{-1} is attributed to the terminal Mo=O in the surface isolated tetrahedral molybdena species. Some researchers [33] hold the view that the Raman frequency at around 950 cm^{-1} is assigned to the terminal Mo=O vibration of polymolybdate species in an octahedral environment. Ekerdt et al. [34] have studied the dispersion behavior of MoO_3 on Al_2O_3 support. They suggest that at low MoO_3 loadings (<2 Mo atoms/nm^2), the isolated MoO_4 tetrahedral species dominate. As the MoO_3 content increases, the isolated MoO_4 tetrahedral species

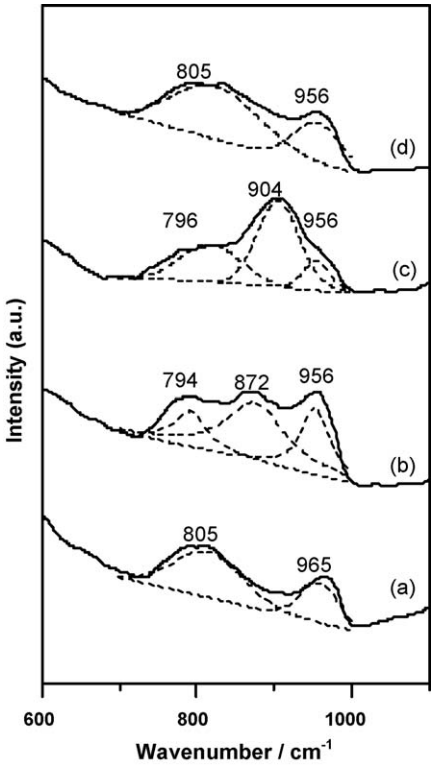

Fig. 5. Raman spectra of $M_xO_y/MoO_3/CeO_2$ samples. (a) 0.8Mo/Ce, (b) Ni/Mo/Ce, (c) Cu/Mo/Ce and (d) Fe/Mo/Ce.

change into polymolybdate octahedral species and the frequency of terminal Mo=O stretching mode increases with the MoO_3 loadings from 921 to 964 cm^{-1}. Along this line, it seems to suggest that for 0.8Mo/Ce sample, the octahedral polymeric molybdena species are the major ones.

When NiO is added to 0.8Mo/Ce sample (Fig. 5b), two vibration peaks of terminal Mo=O bonds are observed at 872 and 956 cm^{-1}. The peak at 956 cm^{-1}, which is very close to the vibration frequency of Mo=O terminal in 0.8Mo/Ce sample, could be attributed to the Mo=O vibration in octahedral polymeric molybdena species. The peak at about 872 cm^{-1} is 93 cm^{-1} lower than that of 0.8Mo/Ce sample, indicating the involvement of Ni^{2+} ions leads to the strong distortion of coordination environment of some Mo atoms in Ni/Mo/Ce sample. As reported elsewhere [35], the structure of molybdena species is tightly correlated to the frequency of Mo–O vibration. According to the theoretic calculation of Hardcastle and Wachs [35], the Raman frequency of Mo–O bonds in perfect MoO_4 tetrahedral structure should be 858 cm^{-1}. The peak at 872 cm^{-1} is only 14 cm^{-1} higher, implying the surface molybdena species are nearly regular MoO_4 tetrahedral structures. All these results indicate that two kinds of molybdena species exist on the surface of Ni/Mo/Ce sample, i.e., tetrahedrally and octahedrally coordinated ones. After addition of CuO (Fig. 5c), the wave number of terminal Mo=O are observed at ~904 and 956 cm^{-1}. Similar with Ni/Mo/Ce sample, the peak at 956 cm^{-1} in Cu/Mo/Ce sample could be attributed to the Mo=O vibration in octahedrally coordinated molybdena species, while the peak at ~904 cm^{-1} is 46 cm^{-1} higher than the frequency of Mo–O bonds in perfect MoO_4 tetrahedral structures (858 cm^{-1}), indicating the structure of these parts of molybdena species might be between tetrahedrally and octahedrally coordinated ones, i.e. a highly distorted tetrahedral structure. While for Fe/Mo/Ce sample (Fig. 5d), there is no obvious change of the frequency of Mo=O terminals compared with 0.8Mo/Ce sample, implying that the existence of Fe^{3+} has very slight effect on the coordinative environment of Mo^{6+} ions and the molybdena species keep octahedrally coordinated structure. Consequently, it seems to predict that the effects of addition of copper, nickel or ferric oxide on the surface structure are different and the intensities of the interaction between the metal oxides and molybdena species could be listed as: Ni/Mo/Ce > Cu/Mo/Ce > Fe/Mo/Ce.

The quantitative analysis has been tentatively employed for the samples as shown in Fig. 5, and the similar treatment has been reported elsewhere [36]. According to the calculation, the peak area ratio of Mo–O–X/Mo=O terminals is about 2.00 for 0.8Mo/Ce sample, and the ratios are 0.21, 0.58 and 2.22 for Ni/Mo/Ce, Cu/Mo/Ce and Fe/Mo/Ce, respectively. The result shows that the proportion of Mo–O–X decreases sharply after addition of NiO or CuO, also implying that the NiO (CuO) has strong effects on the structures of molybdena species on the surface of CeO_2 and may lead to the destroy of Mo–O–Mo bonds and the formation of isolated molybdena species. Moreover, the ratio of Ni/Mo/Ce is less than Cu/Mo/Ce, also indicating the NiO has stronger interaction with molybdena species.

Some researchers studied the Raman spectroscopy of $M^{2+}O$–MoO_3 bimetallic oxides supported on various supports and our result is also supported by their studies. Prins et al. studied the $NiMo/SiO_2$ catalysts and found that compared with Mo/SiO_2 sample with Mo=O frequency at 973 and 957 cm^{-1}, the $NiMo/SiO_2$ sample has an additional Mo=O vibration at lower frequency (~905 cm^{-1}) [37]. Liu et al. found that for ZnO/MoZr system, with the ZnO loading increases, the Mo=O frequency shifted to lower wave number which is attributed to the formation of isolated molybdena species [38].

The possible reason may be the difference in the structures of surface species: As Fig. 4b shows, for Ni/Mo/Ce sample, each Ni^{2+} has one capping oxygen ion for charge compensation, so the coordinative oxygen ions of Ni^{2+} form a nearly normal tetrahedron, which is a symmetrical stable structure, i.e., the interaction between Ni^{2+} and the capping oxygen ions linked with Mo^{6+} is fairly strong. The schematic structures of polymeric molybdena species could be schemed as Fig. 6a [39]. After addition of NiO, the strong interaction between Ni^{2+} and molybdena species leads to the following two effects as Fig. 6b shows:

1. Some of the Mo–O–Mo bonds are destroyed and the polymerization degree of molybdena species decreases, thus the structures change from polymeric octahedral ones into isolated tetrahedral ones.
2. The bond intensities of Mo=O decrease and its Raman frequency shifts to lower wave number, which makes the MoO_4 structures are nearly regular tetrahedral structure.

For Cu/Mo/Ce sample, as discussed above, the molybdena species in Cu/Mo/Ce sample are highly distorted tetrahedral structure, indicating the interaction between Cu^{2+} and molybdena species is lower than that of between Ni^{2+} and molybdena species. The possible reasons may be as following:

1. Considering that the Ni^{2+} has smaller ion radius (69 pm) than Cu^{2+} (73 pm) [40], thus the electrostatic attraction between Ni^{2+} and molybdena species is stronger than that of between Cu^{2+} and molybdena species.
2. The tetrahedral crystal field stabilization energies (CFSE) of Ni^{2+} (outer electronic configuration: $3d^8$) and Cu^{2+} (outer electronic configuration: $3d^9$) are $-3.55\,Dq + 3P$ and $-1.78\,Dq + 4P$ (where P is the pairing energy), respectively [41], indicating that the tetrahedrally coordinated Ni^{2+} is more stable than Cu^{2+}.

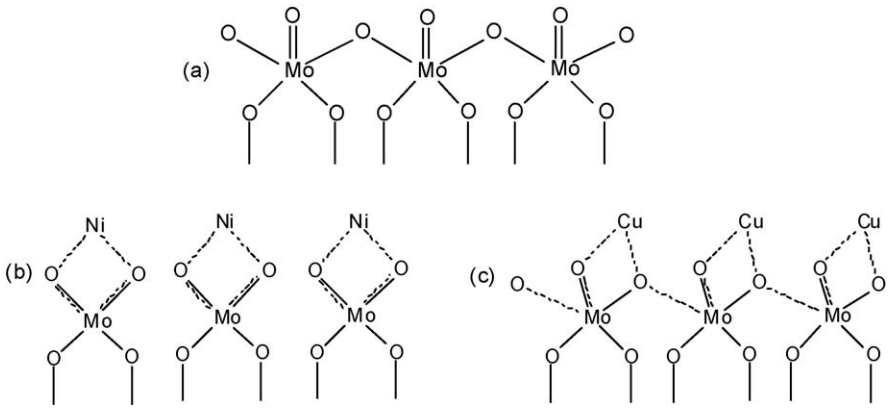

Fig. 6. Schematic drawing of the structures of molybdena species for the surface of (a) 0.8Mo/Ce, (b) Ni/Mo/Ce and (c) Cu/Mo/Ce.

Thus, the interaction between Cu^{2+} and molybdena species in Cu/Mo/Ce is weaker than that of between Ni^{2+} and molybdena species in Ni/Mo/Ce. As shown in Fig. 6c, the Mo–O–Mo bonds may not be destroyed completely in Cu/Mo/Ce sample, so the octahedral molybdena species could not transform to tetrahedral ones completely, leading to the formation of highly distorted tetrahedral molybdena species with weak interactions between MoO_4 tetrahedral species, which could be thought as the intermediate configuration between octahedral and tetrahedral structures.

While for Fe/Mo/Ce samples, each Fe^{3+} needs 3/2 capping oxygen ions in average for charge compensation. At low Fe^{3+} loadings, the coordinative environment of Fe^{3+} might be a highly distorted unstable structure, i.e., the interaction between Fe^{3+} and the capping oxygen ions of Mo^{6+} ions is weak. Therefore, the two effects mentioned above could not work, so the frequency of Mo=O keeps almost unchanged and the molybdena species retain the octahedral structures, just as that of 0.8Mo/Ce sample shown in Fig. 6a.

3.4. NH_3-adsorbed in situ FT-IR

Ammonia adsorption FT-IR results in N–H bending region (ranging from 1700 to 1100 cm^{-1}) of 0.8Mo/Ce, Ni/Mo/Ce, Cu/Mo/Ce and Fe/Mo/Ce at 50 °C are presented in Fig. 7. For 0.8Mo/Ce (Fig. 7a), a strong peak at 1437 cm^{-1} ascribed to the asymmetry deformation vibration of ammonia cation NH_4^+ can be detected, which suggests that ammonia are protonated at the Brønsted acid sites of the sample [42–46]. The weak peak at 1255 cm^{-1} is attributed to the symmetry deformation mode $\delta_{sym}NH_3$, indicating the existence of Lewis acid sites (although very few) on the polymeric molybdena species, i.e., some ammonia molecules adsorb on coordinatively unsaturated Mo^{6+} ions [42–46]. The peak area of ammonia adsorption on Brønsted acid sites is much larger than that on Lewis acid sites, indicating the Brønsted acid sites are the main acid sites on the surface of 0.8Mo/Ce sample at low temperatures.

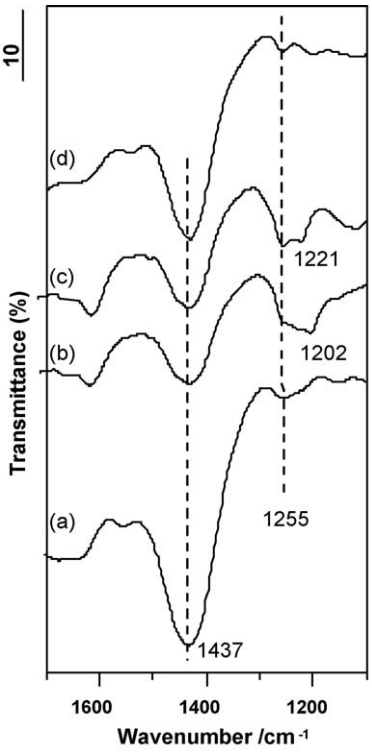

Fig. 7. Ammonia adsorption FT-IR spectra of $M_xO_y/MoO_3/CeO_2$ samples at 50 °C. (a) 0.8Mo/Ce, (b) Ni/Mo/Ce, (c) Cu/Mo/Ce and (d) Fe/Mo/Ce.

For Ni/Mo/Ce and Cu/Mo/Ce (Fig. 7b and c, respectively) samples, it can be seen that the peaks of NH_3 adsorption on Brønsted acid sites (~1437 cm^{-1}) and Lewis acid sites (~1200 cm^{-1}) are both obviously observed, indicating that there are abundant Brønsted acid sites as well as Lewis acid sites on the surface of the samples. Especially, it is worth noting that the Lewis acid sites on the surface of these two samples are different. For Ni/Mo/Ce sample, two peaks at 1255 and 1202 cm^{-1} can be observed, indicating the existence of two different Lewis acid sites. The peak at 1255 cm^{-1} can also be observed in 0.8Mo/Ce sample and should be the same Lewis acid sites with that in 0.8Mo/Ce (marked as L1). While the peak at 1202 cm^{-1}, only be detected in Ni/Mo/Ce, should be attributed to NH_3 adsorption on a new Lewis acid sites (marked as L2), implying the formation of new molybdena species on the surface of Ni/Mo/Ce sample. For Cu/Mo/Ce sample, similar peaks can be observed, except the wave number of the peak at 1202 cm^{-1} shifts to 1220 cm^{-1}. As the formation mechanism of the new Lewis acid sites in Cu/Mo/Ce is similar as that in Ni/Mo/Ce, we also marked it as L2. According to the discussion above, we know that with the addition of NiO or CuO, part of the polymeric molybdena species will transform to isolated regular tetrahedral or highly distorted tetrahedral molybdena species (Fig. 6), respectively. So, it is reasonable to suggest that the formation of the new Lewis acid sites on the surface of samples should be related to the creation of the tetrahedral molybdena species, which also indicates that the interaction between Ni^{2+}(Cu^{2+}) and molybdena species is very strong.

While for Fe/Mo/Ce sample, the profile of ammonia adsorption FT-IR spectra (Fig. 7d) is almost similar with that of 0.8Mo/Ce (Fig. 7a), i.e., the Fe/Mo/Ce sample has a large amount of Brønsted acid sites and very few Lewis acid sites at low temperatures, indicating that the polymeric molybdena species are the primary ones on the surface of Fe/Mo/Ce sample. The result also implies that interaction between Fe^{3+} and molybdena species is extremely weak.

For further comparison of the acid sites in the four samples, the results of NH_3-adsorbed in situ FT-IR at different temperatures are presented in Fig. 8. It can be seen that the desorption temperatures of NH_3 adsorption on Brønsted acid sites of 0.8Mo/Ce (Fig. 8a) and Fe/Mo/Ce (Fig. 8d) are both at about 250 °C, implying that the interaction between Fe^{3+} and molybdena species is very weak. Namely, the Fe/Mo/Ce sample has similar Brønsted acid intensities with 0.8Mo/Ce. For Ni/Mo/Ce (Fig. 8b) and Cu/Mo/Ce (Fig. 8c) samples, the desorption temperatures on Brønsted acid sites are both at about 200 °C. However, the acid intensities of Lewis acid sites of Ni/Mo/Ce and Cu/Mo/Ce samples are different. (1) The ammonia on L1 sites desorbs completely at 150 °C in Cu/Mo/Ce catalyst, but only partly desorbs in Ni/Mo/Ce catalyst at the same temperature. (2) The ammonia adsorption on the L2 sites is more stable than that on L1 sites and the desorption temperature is higher for Ni/Mo/Ce sample (>400 °C) than that for Cu/Mo/Ce sample (~350 °C). Overall, the result indicates that the intensity of Lewis acids in Ni/Mo/Ce is stronger than that in Cu/Mo/Ce sample. It can be explained by the structures of molybdena species in Ni/Mo/Ce and Cu/Mo/Ce samples. As the interaction of Ni^{2+} and molybdena species is stronger than that of between Cu^{2+} and molybdena species, the MoO_4 tetrahedra in Ni/Mo/Ce are isolated regular tetrahedral structures (Fig. 6b), which is easy to coordinatively adsorb NH_3 molecules and the NH_3 adsorption on the Lewis acid sites of Ni/Mo/Ce is very stable. While the molybdena species in Cu/Mo/Ce sample are highly distorted tetrahedral structures due to the weak interaction between MoO_4 tetrahedral ones (Fig. 6c), which makes it difficult for ammonia to coordinatively adsorb on the Lewis acid sites. Thus, it can be concluded that the intensities of Lewis acid sites increase with the intensities of interaction between metal oxides and molybdena

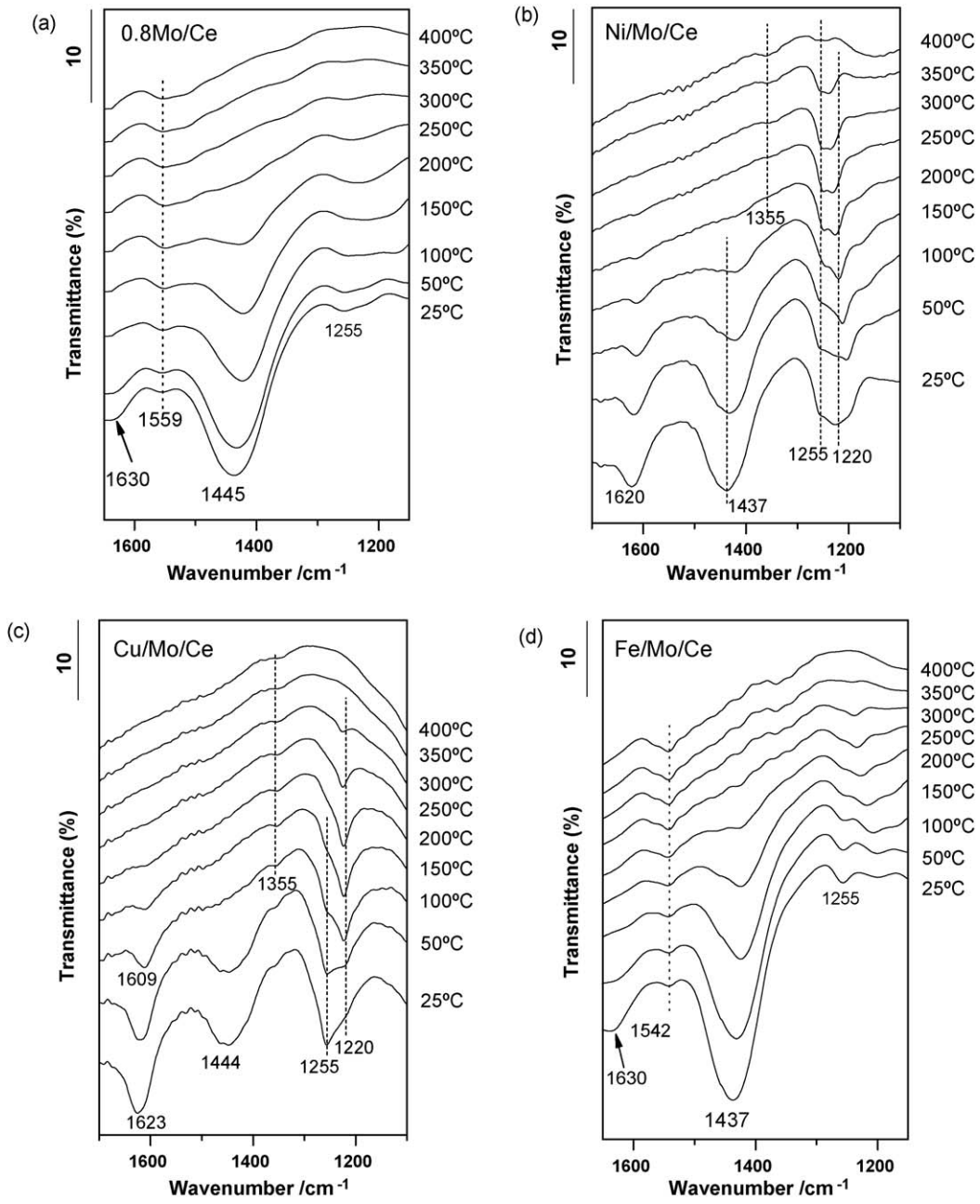

Fig. 8. In situ ammonia adsorption FT-IR spectra of (a) 0.8Mo/Ce, (b) Ni/Mo/Ce, (c) Cu/Mo/Ce and (d) Fe/Mo/Ce.

species, i.e., the intensities of surface Lewis acid sites has the following order: Ni/Mo/Ce > Cu/Mo/Ce > Fe/Mo/Ce.

It is interesting to be noted that a group of weak peaks appear at 1559 cm^{-1} in FT-IR spectra for 0.8Mo/Ce sample. For Fe/Mo/Ce sample, similar peaks appear at about 1542 cm^{-1}. According to the literature [46], the peak should be attributed to the $\delta_{sym}NH_3$ of the $-NH_3^+$ group. The results indicate that the adsorbed ammonia decomposed at the surface and formed NH_3^+ radical ions. With the increase of temperature, the peak intensity of NH_4^+ decreases gradually and the peak intensity of $-NH_3^+$ species increases simultaneously, indicating the $-NH_3^+$ may form from the decomposition of NH_4^+ adsorbed on the Brønsted acid sites. The intensity keeps constant when the temperature is higher than 250 °C, which is also the desorption temperature of the ammonia adsorption on Brønsted acid sites. As the Lewis acid sites on the sample are extremely weak, it is concluded that the peaks are attributed to the decomposition products of NH_4^+ adsorbed on Brønsted acid sites.

Ni/Mo/Ce and Cu/Mo/Ce samples consist both Brønsted and Lewis acid sites on the surface. A group of new peaks at about 1355 cm^{-1} can be observed at temperature higher than 100 °C and its intensity increases with the weaken of ammonia desorption on Lewis acid sites, as can be seen in FT-IR spectra. It is concluded that the peaks are the decomposition products of NH_3 adsorbed on Lewis acid sites. According to the literatures [45,46], the peak is the wagging vibration of NH_2 species, so we temporarily attribute the peak to the NH_2 species adsorbed on the Lewis acid sites. However, the peaks attributed to the decomposition of NH_4^+ adsorbed on Brønsted acid sites do not appear in FT-IR spectra. It can be explained from the competition adsorption of ammonia on Brønsted and Lewis acid sites. The adsorption/desorption and decomposition/composition processes are both irreversible

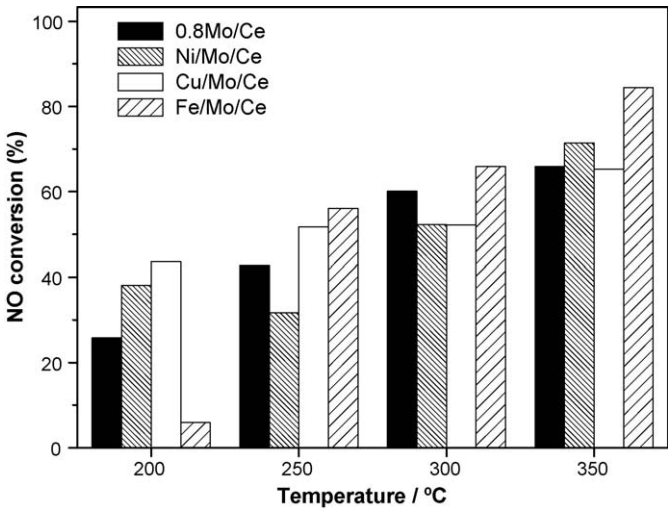

Fig. 9. The NO conversion for different catalysts in "NO + NH_3 + O_2" reaction.

processes. As can be seen from the FT-IR spectra, the ammonia desorption temperature on Brønsted acid sites is about 200 °C, while no obvious ammonia desorption on L2 Lewis acid sites can be observed before 250 °C. The L2 sites can re-adsorb the ammonia molecules desorbed from Brønsted acid sites, thus hinder the decomposition of ammonia at Brønsted acid sites.

3.5. Activity of NO + NH_3 + O_2 reaction

Fig. 9 gives the NO conversion of all the samples for the selective catalytic reduction (SCR) of NO by NH_3 as a function of temperature. It can be seen: (1) at low temperature (200 °C), the NO conversions of Ni/Mo/Ce and Cu/Mo/Ce are higher than that of 0.8Mo/Ce and Fe/Mo/Ce catalysts; (2) when the temperature reaches to 300 °C, the activities of 0.8Mo/Ce and Fe/Mo/Ce enhance significantly compared with 200 °C, while the activity increments of Ni/Mo/Ce and Cu/Mo/Ce samples are much less. The NO conversions of 0.8Mo/Ce and Fe/Mo/Ce are obviously higher than those of Ni/Mo/Ce and Cu/Mo/Ce; (3) With the further increase of temperature to ~350 °C, the activities of Ni/Mo/Ce and Cu/Mo/Ce increase obviously to almost the same NO conversion with 0.8Mo/Ce samples.

Many researchers have studied the mechanism of "NO + NH_3 + O_2" reaction and all authors agree that ammonia is strongly adsorbed and activated on the surface acid sites of the catalysts, later reacting with gas-phase or weakly adsorbed NO. However, whether Brønsted or Lewis acid sites are active sites for this reaction is still controversial [12,13,47–55]. Especially, some computational methods indicated that the reaction occurring on either Lewis acid or Brønsted acid sites is reasonable and the corresponding mechanism is suggested [47–49]. However, they do not use real catalysts and do not point out in which condition the acid sites can promote the reaction process.

On the bases of the literatures and our present works, the reaction activities at different temperatures should be related to the acidity properties of the catalysts. According to the results of NH_3-adsorbed in situ FT-IR, the ammonia adsorption and decomposition on Brønsted and Lewis acid sites can be schemed as Fig. 10. Recall the discussion about NH_3-adsorbed in situ FT-IR, at low temperature (~200 °C), the ammonia molecules on L1 sites of Cu/Mo/Ce and Ni/Mo/Ce catalysts desorb obviously to form NH_2 species. At this temperature, the Ni/Mo/Ce and Cu/Mo/Ce have much higher activities than 0.8Mo/Ce and Fe/Mo/Ce. Thus, the NH_2 species should be the active intermediate for the reaction and the L1 acid site is the main active site at low temperature. It can be seen that the peaks of NH_2 species of Ni/Mo/Ce sample are very weak below 200 °C. Thus, the NO conversion of Ni/Mo/Ce catalyst is lower than that of Cu/Mo/Ce. At middle range of temperature (~250–300 °C), the ammonia on Brønsted acid sites of 0.8Mo/Ce and Fe/Mo/Ce catalysts desorbs completely and the peaks of $-NH_3^+$ species reach to maximum at ~250 °C. Accordingly, the catalytic activities of these two catalysts increase significantly from 200 to 300 °C, indicating the $-NH_3^+$ species might be the

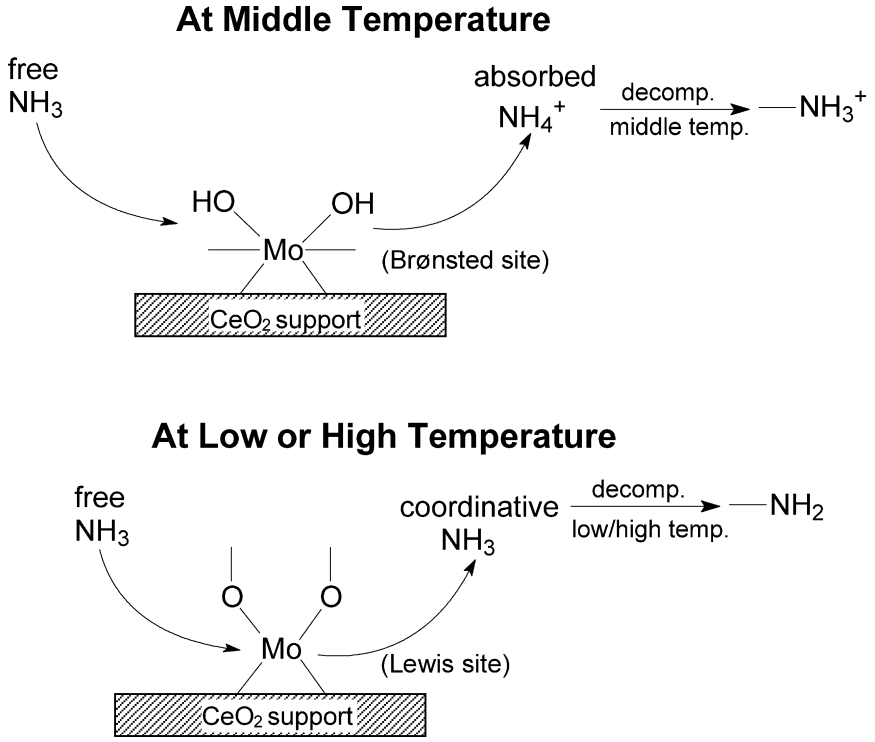

Fig. 10. Schematic drawing of ammonia adsorption and decomposition on Brønsted and Lewis acid sites.

active intermediate for "$NO + NH_3 + O_2$" reaction and the Brønsted acid site should be the main active site at middle temperature. With the further increase of temperature to 350 °C, the ammonia molecules adsorbed on L2 Lewis acid sites begin to decompose to form NH_2 species. At this temperature, the activities of Ni/Mo/Ce and Cu/Mo/Ce increase obviously to almost the same NO conversion with 0.8Mo/Ce sample, indicating the NH_2 species formed on Lewis acid sites should be active sites for "$NO + NH_3 + O_2$" reactions at high temperatures. However, the Fe/Mo/Ce sample has much higher activity than the other three samples, which might be attributed to the promotion effects of Fe species on the NO SCR reactions [56].

4. Conclusions

1. For $M_xO_y/MoO_3/CeO_2$ (M = Ni, Cu, Fe) samples, the formation of monolayer molybdena species on the surface of ceria supports could effectively influence the properties of M_xO_y/CeO_2 samples. For example, the reduction of dispersed M_xO_y species in $M_xO_y/MoO_3/CeO_2$ is more difficult than that of corresponding M_xO_y/CeO_2 samples.
2. The additions of NiO, CuO and Fe_2O_3 have different effects on the structures of molybdena species, i.e., isolated regular tetrahedral, high distorted tetrahedral and polymeric octahedral structures, respectively. The different states of the dispersed molybdena species should result from the different intensities of interaction between metal oxides and molybdena species, which could be listed as: Ni/Mo/Ce > Cu/Mo/Ce > Fe/Mo/Ce.
3. For M/Mo/Ce samples, the surface acid intensities of Lewis acid sites are influenced by the surface structures of molybdena species, which also exhibit the same order: Ni/Mo/Ce > Cu/Mo/Ce > Fe/Mo/Ce, i.e., the Ni/Mo/Ce sample has the strongest Lewis acid intensity and the Fe/Mo/Ce sample has the weakest Lewis acid intensity.
4. The activity of "$NO + NH_3 + O_2$" reaction is tightly related with acidity properties of the catalysts. For our $M_xO_y/MoO_3/CeO_2$ system, the relationship between acid sites and "$NO + NH_3 + O_2$" reactivity is as following: at low temperature, the weak Lewis acid sites (L1) are the main active sites for "$NO + NH_3 + O_2$" reaction; at middle temperature, Brønsted acid sites are the primary active sites; while at high temperature, the strong Lewis acid sites (L2) can also promote the reaction.

Acknowledgements

This work was financially supported by the National Natural Science Foundation of China (No. 20873060), the National Basic Research Program of China (2004CB719502) and the Project of Jiangsu Innovation Talent (BK2008001). Kind assistance offered by Prof. Zhong Qin's group (School of Chemical Engineering, Nanjing University of Science and Technology) is also gratefully acknowledged.

References

[1] H. Schneider, U. Scharf, A. Wokaun, A. Baiker, J. Catal. 146 (1994) 545–556.
[2] L. Ilieva, G. Pantaleo, I. Ivanov, A.M. Venezia, D. Andreeva, Appl. Catal. B: Environ. 65 (2006) 101–109.
[3] H.O. Zhu, J.R. Kim, S.K. Ihm, Appl. Catal. B: Environ. 86 (2009) 87–92.
[4] B. Wen, M.Y. He, Appl. Catal. B: Environ. 37 (2002) 75–82.
[5] F. Amano, S. Suzuki, T. Yamamoto, T. Tanaka, Appl. Catal. B: Environ. 64 (2006) 282–289.
[6] L.J. Liu, B. Liu, L.H. Dong, J. Zhu, H.Q. Wan, K.Q. Sun, B. Zhao, H.Y. Zhu, L. Dong, Y. Chen, Appl. Catal. B: Environ. 90 (2009) 578–586.
[7] L.J. Liu, Y. Chen, L.H. Dong, J. Zhu, H.Q. Wan, B. Liu, B. Zhao, H.Y. Zhu, K.Q. Sun, L. Dong, Y. Chen, Appl. Catal. B: Environ. 90 (2009) 105–114.
[8] X.L. Tang, J.M. Hao, W.G. Xu, J.H. Li, Catal. Commun. 8 (2007) 329–334.
[9] G. Qi, R.T. Yang, Appl. Catal. B: Environ. 44 (2003) 217–225.
[10] Z. Huang, Z. Zhu, Z. Liu, Appl. Catal. B: Environ. 39 (2002) 361–368.
[11] E. García-Bordejé, J.L. Pinilla, M.J. Lázaro, R. Moliner, Appl. Catal. B: Environ. 66 (2006) 281–287.
[12] G. Ramis, G. Busca, F. Bregani, P. Forzatti, Appl. Catal. 64 (1990) 259–278.
[13] J.A. Dumesic, N.Y. Topsøe, H. Topsøe, Y. Chen, T. Slabiak, J. Catal. 163 (1996) 409–417.
[14] Ch. Fountzoula, N. Spanos, H.K. Matrails, Ch. Kordulis, Appl. Catal. B: Environ. 35 (2002) 295–304.
[15] W.J. Chun, K. Asakura, Y. Iwasawa, J. Phys. Chem. B 102 (1998) 9006–9014.
[16] I. Nova, L. Lietti, L. Casagrande, L. DallÍAcqua, E. Giamello, P. Forzatti, Appl. Catal. B: Environ. 17 (1998) 245–258.
[17] M. Del Arco, C. Martín, V. Rives, V. Sanchez-Escribano, G. Ramis, G. Busca, V. Lorenzelli, P. Malet, J. Chem. Soc., Faraday Trans. 89 (1993) 1071–1078.
[18] K.V.R. Chary, T. Bhaskar, G. Kishan, V. Vijayakumar, J. Phys. Chem. B 102 (1998) 3936–3940.
[19] S. Gunther, M. Marsi, A. Kolmakov, M. Kiskinova, M. Noeske, E. Taglauer, G. Mestl, U.A. Schubert, H. Knozinger, J. Phys. Chem. B 101 (1997) 10004–10011.
[20] Y. Zhao, R. Prins, J. Catal. 229 (2005) 213–226.
[21] H.Q. Wan, Z. Wang, J. Zhu, X.W. Li, B. Liu, F. Gao, L. Dong, Y. Chen, Appl. Catal. B: Environ. 79 (2008) 254–261.
[22] L. Dong, Y. Chen, J. Chem. Soc., Faraday Trans. 92 (1996) 4589–4593.
[23] Y. Li, B.C. Zhang, X.L. Tang, Y.D. Xu, W.J. Shen, Catal. Commun. 7 (2006) 380–386.
[24] P. Zimmer, A. Tschöpe, R.J. Birringer, J. Catal. 205 (2002) 339–345.
[25] M.M. Mohamed, Spectrochim. Acta 51A (1995) 1–9.
[26] C.H. Wang, H.S. Weng, Appl. Catal. A: Gen. 170 (1998) 73–80.
[27] N.R.E. Radwan, E.A. El-Sharkawy, A.M. Youssef, Appl. Catal. A: Gen. 281 (2005) 93–106.
[28] S. Minico, S. Scire, C. Crisafulli, R. Maggiore, S. Gahvagno, Appl. Catal. B: Environ. 28 (2000) 245–251.
[29] G. Mestl, T.K.K. Srinivasan, Catal. Rev. Sci. Eng. 40 (1998) 451–570.
[30] B. Samaranch, P.R. de la Piscina, G. Clet, M. Houalla, N. Homs, Chem. Mater. 18 (2006) 1581–1586.
[31] K.D. Chen, S. Xie, E. Iglesia, A.T. Bell, J. Catal. 189 (2000) 421–430.
[32] K.Y.S. Ng, E. Gulari, J. Catal. 92 (1985) 340–354.
[33] P. Dufresne, E. Payen, J. Grimblot, J.P. Bonnelle, J. Phys. Chem. 85 (1981) 2344–2351.
[34] C.C. Williams, J.G. Ekerdt, J.M. Jehng, F.D. Hardcastle, I.E. Wachs, J. Phys. Chem. 95 (1991) 8791–8797.
[35] F.D. Hardcastle, I.E. Wachs, J. Raman Spectrosc. 21 (1990) 683–691.
[36] A. Montesinos-Castellanos, T.A. Zepeda, Micropor. Mesopor. Mater. 113 (2008) 146–162.
[37] R. Cattaneo, T. Shido, R. Prins, J. Catal. 185 (1999) 199–212.
[38] Z. Liu, L. Dong, W. Ji, Y. Chen, J. Chem. Soc., Faraday Trans. 94 (1998) 1137–1142.
[39] A. Christodoulakis, E. Heracleous, A.A. Lemonidou, S. Boghosian, J. Catal. 242 (2006) 16–25.
[40] J.G. Speight, Lange's Handbook of Chemistry, 16th edition, CD&W Inc., Laramie, Wyoming, 2004.
[41] J.E. Huheey, Inorganic Chemistry Principles of Structure and Reactivity, 2nd edition, Prentice Hall, 1987.
[42] L. Dall'Acqua, I. Nova, L. Lietti, G. Ramis, G. Busca, E. Giamello, Phys. Chem. Chem. Phys. 2 (2000) 4991–4998.
[43] M.A. Centeno, I. Carrizosa, J.A. Odriozola, J. Alloy Compd. 323–324 (2001) 597–600.
[44] N. Naito, N. Katada, M. Niwa, J. Phys. Chem. B 103 (1999) 7206–7213.
[45] K. Hadjiivanov, Appl. Surf. Sci. 135 (1998) 331–338.
[46] J.M.G. Amores, V.S. Escribano, G. Ramis, G. Busca, Appl. Catal. B: Environ. 13 (1997) 45–58.
[47] K. Jug, T. Homann, T. Bredow, J. Phys. Chem. A 108 (2004) 2966–2971.
[48] M. Anstrom, N.Y. Topsøe, J.A. Dumesic, J. Catal. 213 (2003) 115–121.
[49] A. Vittadini, M. Casarin, A. Selloni, J. Phys. Chem. B 109 (2005) 1652–1655.
[50] Z. Huang, Z. Liu, X. Zhang, Q. Liu, Appl. Catal. B: Environ. 63 (2006) 260–265.
[51] D.A. Pena, B.S. Uphade, P.G. Smirniotis, J. Catal. 221 (2004) 421–431.
[52] M. Kobayashi, K. Miyoshi, Appl. Catal. B: Environ. 72 (2007) 253–261.
[53] B. Huang, R. Huang, D. Jin, D. Ye, Catal. Today 126 (2007) 279–283.
[54] G. Qi, R.T. Yang, R. Chang, Appl. Catal. B: Environ. 51 (2004) 93–106.
[55] R.Q. Long, et al. Appl. Catal. B: Environ. 24 (2000) 13–21.
[56] N. Apostolescu, B. Geiger, K. Hizbullah, M.T. Jan, S. Kureti, D. Reichert, F. Schott, W. Weisweiler, Appl. Catal. B: Environ. 62 (2006) 104–114.